

Thermodynamics and Phase Stability in the Ga–N System

J. Unland^a, B. Onderka^a, A. Davydov^b, R. Schmid-Fetzer^{a,*}

^a *Institute of Metallurgy, Technical University of Clausthal, Robert-Koch-Str. 42, D-38678 Clausthal-Zellerfeld, Germany*

^b *NIST, Metallurgy Division, Gaithersburg, USA*

Received 25 June 2002; accepted 6 May 2003

Communicated by K. Nakajima

Abstract

The decomposition of GaN powder was studied experimentally using two different customized thermogravimetric methods, dynamic oscillation TGA, and isothermal stepping TGA for a higher resolution of the decomposition start. A reproducible mass gain at slightly lower temperature suggests the equilibrium temperature to be at 1110 ± 10 K under 1 bar of nitrogen. A CALPHAD type thermodynamic analysis of all available phase equilibrium and thermodynamic data is performed. This includes the determination of the absolute entropy of GaN, 30 ± 4 J/mol K, based on a Debye–Einstein-analysis of the experimental data on the heat capacity. An explicit equation for the fugacity–pressure relation of nitrogen, $f(P)$, is developed, which is useful for the conversion of complex phase diagram calculation output. This is crucial because f can be several orders of magnitude higher than P for the high pressures encountered during GaN decomposition. Based on the consistent thermodynamic description, developed for the Ga–N system, all thermodynamic data and various phase diagrams are calculated. They indicate a good overall agreement between the different types of experimental data (calorimetric, vapor pressure, phase equilibrium). The high pressure part of the decomposition pressure of GaN is actually predicted from the thermodynamic model in good agreement with the experimental data.

© 2003 Elsevier B.V. All rights reserved.

Keywords: A1. Phase diagram; A1. Thermodynamics; B1. Nitrides; B2. Semiconducting III–V materials

1. Introduction

The best researched group III-Nitride semiconductor is GaN, mainly because this was the first material with an exceptional bright blue light emission in LEDs and lasers. The technology of fabrication of such optoelectronic or high speed

electronic devices involve processes that require the direct contact of the solid, liquid and gas phase near equilibrium conditions [1–3]. Knowledge of the thermodynamic phase stabilities and of the pressure–temperature–composition phase diagram is important for an understanding of the boundary conditions of a variety of processing steps. This is even true for non-equilibrium processing routes since the distance from or driving force to the equilibrium state should be known quantitatively. For device applications it is important to clarify the stable and the unstable compositions of III–N

*Corresponding author. Tel.: +49-5323-72-2150; fax: +49-5323-72-3120.

E-mail address: schmid-fetzer@tu-clausthal.de
(R. Schmid-Fetzer).

materials, since thermal degradation during device processing or operation may be caused in part by sublimation and/or thermal decomposition. Therefore consistent thermodynamic models of III-N binary system are indispensable which combine all available thermodynamic properties and phase equilibria and allow calculation of reasonable and internally consistent estimates of missing properties, as well as the thermodynamic driving forces of reactions.

Since the first presentation of a CALPHAD type assessment of the Ga–N system [4,5] a number of important new experimental data became avail-

able. A compilation of the published experimental work on GaN, mainly decomposition and formation, under a nitrogen atmosphere can be found in Table 1. A number of publications ([6,16,23–31]) deal with experimental data on the GaN stability under NH_3 or mixtures containing NH_3 . Published thermodynamic data, like the enthalpy of formation of GaN, are summarized in Table 2. A detailed discussion of these data will be given later. A review of related species important for vapor phase epitaxy is given by Przhevskii et al. [37].

The purpose of this work is two-fold: (i) to present new experimental results on the

Table 1
Summary of GaN stability experiments with samples heated in nitrogen (N_2)

Ref. Year [Ref.#]	F,D,S ^a	Method of detection	Temp. range [K]	Pressure range [bar]
1940 [6]	D	Not given	1273	1
1956 [7]	D ^b	Mass loss	1170–1430	1
1962 [8]	D	N_2 -pressure measurement	685–1268	1.5×10^{-6} –0.63
1965 [9]	D ^c	Torsion effusion	1189	1×10^{-5}
1970 [10]	D	Not given	1873	700
1974 [11]	D ^d	Thermogravimetry, mass-spectrometry	298–1273	1×10^{-9} – 1×10^{-7}
1974 [12]	No D ^e	Mass loss, microscopy	1273	1
1975 [13]	D	Microscopy	1113–1523	100 – 1×10^4
	F	Mass gain	1273–1473	100 – 1×10^4
	S	Not given	1473	8×10^3
1976 [14]	D	Not given	1243	1
1977 [15]	F	Not given	1023	100
1983 [16]	D	Color-change; mass loss	1023–1343	1 ^f
1984 [17]	D	XRD ^g	1343–1963	100 – 2×10^4
		Color-change; microscopy	1773–2573	2.5×10^4 – 6×10^4
	S	Not given	1773	1.6×10^4
1991 [18]	S	Thermal conductivity	1473–1853	1.3×10^3 – 1.43×10^4
1993 [19]	F	Not given	1633–1673	9.5×10^3 – 1.7×10^4
1995 [20]	S	Thermal conductivity	1680–1820	6×10^3 – 1.1×10^4
1996 [21]	D ^d	Mass-spectrometry	298–1373	2×10^{-11} – 1×10^{-9}
1998 [22]	D ^c	In situ hot stage microscopy	973–1073	1 ⁱ
1998 [23]	No D ^h	SEM	1223	0.1
1999 [24]	D	In situ laser reflectometry	1323	1 ^j
This work	D, F	STA	973–1323	1

^a F = Formation, starting with Ga, ($2\text{Ga(l)} + \text{N}_2(\text{g}) \rightarrow 2\text{GaN(s)}$), D = Decomposition, starting with GaN, ($2\text{GaN(s)} \rightarrow 2\text{Ga(l)} + \text{N}_2(\text{g})$), S = Solubility of N in Ga(l).

^b Reported as vaporization of GaN(s).

^c Starting with GaN(s) + Ga(l).

^d Conditions far from equilibrium, pressure at sample unclear.

^e No decomposition at 1273 K for 20 min.

^f Unclear gas composition and pressure.

^g Only for undecomposed GaN; method for Ga(l) is not given.

^h No decomposition at 1223 K for 15 min.

ⁱ $\text{N}_2(95\%) + \text{H}_2(5\%)$.

^j $\text{N}_2(17\text{--}83\%) + \text{H}_2(83\text{--}17\%)$.

Table 2
Summary of experiments on thermodynamic properties of GaN

Ref. Year [Ref.#]	Method	T [K]	$\Delta_f H_{298}^0$ [kJ/mol] ^a	S_{298}^0 [J/mol K]
1940 [27]	Combustion calorimetry		-104.2 ± 4	
1975 [32]	$C_p(T)$ measurements	55–300		36.9
1975 [13]	Derived from linearized $P(T)$ curves	1223–1473	-157.7	
1979 [33]	$C_p(T)$ measurements	5–300		36.5
1984 [34]	Derived from linearized $P(T)$ curves	1343–1863	-157.7 ± 3	
1999 [35]	$C_p(T)$ measurements	113–1073		
2000 [36]	Drop solution calorimetry	975	-156.8 ± 16	

^aThe mol refers to the formula unit (GaN) throughout this work.

decomposition and formation of GaN powder under pure nitrogen, involving specially adapted techniques of thermogravimetric analysis; and (ii) to use these data and the entity of published experimental information on phase equilibria and thermodynamic properties to develop a completely revised, comprehensive and consistent thermodynamic description of the Ga–N system.

2. Experimental study of GaN powder decomposition

2.1. Experimental setup and sample characterization

Measurement of the decomposition temperature of GaN powder was done using simultaneous thermal analysis (STA) with specially adapted methods described in the following two sections. STA combines differential thermal analysis (DTA) and thermogravimetric analysis (TGA) in a simultaneous experiment. The STA system (Netzsch STA-409) with an SiC resistance furnace (<1850 K) was used under 1 bar of flowing nitrogen. Pure GaN powders were used as samples with a mass of ~ 100 – 200 mg in 0.3 ml open alumina crucibles, 99.7 wt% Al_2O_3 (Netzsch). As a thermal reference material Al_2O_3 powder was used. Details about the materials used can be found in Table 3.

It is vital for these long-time experiments to ensure highest purity of nitrogen in order to avoid the growth of small whiskers of gallium oxide at the upper edge of the sample crucible and thus to

Table 3
Materials used in present experiments

Material	Purity/size	Supplier
N_2 -gas	Purity 5.5 ^a	AGA, Germany
Millipore filters	WPMV200SI	Millipore Co., Bedford, MA, USA
GaN powder	Purity 99.99%	Alfa Aesar, Germany
Al_2O_3 powder	purity 99.997%	Alfa Aesar, Germany

^aSubsequent gas purification with Millipore filters (<1 ppb).

arrive at reproducible data. Previously used soldered copper gas pipes had been replaced by a complete line of stainless-steel pipes and dedicated gas purification (MILLIPORE filters, <1 ppb) was used. The PtRh10-Pt thermocouples of the DTA head of the STA system were calibrated for the melting temperature of pure In (99.99%), Pb(99.998%), Zn(99.999%), Al(99.97%), Ag(99.99%), Au(99.95%) and an overall temperature measurement accuracy was estimated to be ± 2 K.

Before each STA-experiment the cold equipment was evacuated for at least 1 h down to a pressure of 3×10^{-6} bar. After purging with nitrogen the evacuation/purging procedure was repeated two times. The constant flow rate of 50 ml/min of N_2 at 1 bar was controlled by a mass-flow meter (Vögtlin).

The commercial GaN powder samples from Alfa Aesar, with the light gray color typical for the powder material, were characterized before the STA experiments by oxygen analysis and X-ray

diffraction. The oxygen analysis of samples actually used gave 1.44 wt% O, measured by inert gas fusion and infrared absorption of CO (Fisher-Rosemount, NOA 5003). Storage of GaN powder under dry inert gas is mandatory since substantial oxygen pick-up was observed after storing part of the material in air. The amount of nitrogen which remained in the sample after the experiment was measured in the same equipment (Fisher-Rosemount, NOA 5003) by inert gas fusion and heat conductivity detection.

The STA experiments were done by two different customized methods. Dynamic oscillation TGA, and isothermal stepping TGA for a higher resolution of the decomposition start. The term STA is not used in the following since it was found that the simultaneously recorded DTA signal does not show any useful effect, probably because of the low heating rate and the very small amount of material decomposing in the initial stage. The temperature of the DTA reference cell, used for the temperature control, was found to be identical to that of the sample within experimental accuracy.

2.2. Dynamic oscillation TGA-experiments

At the beginning of each experiment the furnace with sample and reference material was first heated to 973 K under constant N₂ flow of 1 bar. The system was thermally equilibrated at 973 K for 20 min.

The dynamic oscillation experiments started from the thermal equilibrium at 973 K. The temperature of the STA furnace was then controlled to emulate the “saw tooth” profile shown in the bottom part of Fig. 1. This profile is generated by (1) a constant heating rate of 1 K/min from 973 K up to 1323 K, (2) directly after reaching 1323 K a cooling down to 973 K with a ramp of 5 K/min, and (3) holding the temperature constant at 973 K for 30 min to ensure that the system has reached its thermal equilibrium. This procedure was repeated two times. At the end the temperature was increased to 1323 K again and kept constant for 8 h, to complete the sample decomposition.

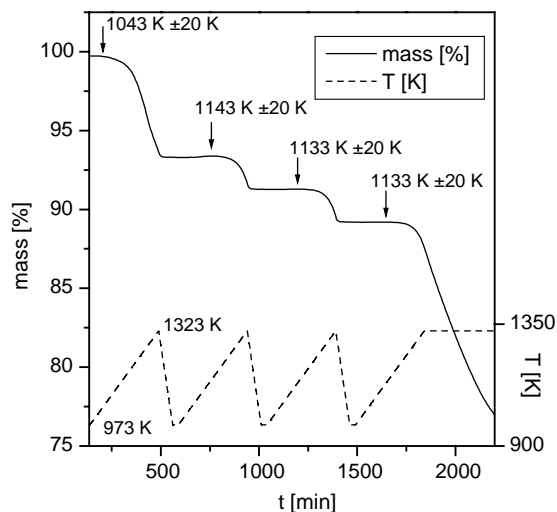


Fig. 1. Typical dynamic oscillation TGA curve showing the mass loss of a GaN powder sample under N₂ at 1 bar for the dynamic method.

2.3. Isothermal stepping TGA

In order to achieve a higher resolution of the initial stage of decomposition an isothermal stepping profile was used for three different GaN samples. At start of each experiment the system was heated up to 1323 K and cooled to 973 K for one time in the same way as described in the dynamic oscillation experiment. This first “saw tooth” was used to produce in situ an amount of gallium metal within the GaN powder. After reaching thermal equilibrium the system was heated up with 1 K/min rate to a selected temperature, typically 1073 K, and kept constant for 2 h. The temperature was then increased to the next selected value, typically 10–25 K higher, and again kept constant for 2 h. Repeating this stepping procedure the temperature was increased up to an upper limit in the range of 1173–1273 K. The continuously recorded mass change was evaluated in the thermally stabilized middle 100 min part of the 120 min time periods at constant temperature.

2.4. Additional experiments

Two additional experiments were performed to obtain more information about the first and final

stages of decomposition and the possible evaporation of Ga(liquid). A sample of GaN was heated up to 1275 K and kept at that temperature for 24 h. The same procedure was repeated separately with pure gallium.

2.5. Results

The mass loss curve for the heating rate of 1 K/min displays an exponential shape around the GaN decomposition, as seen in Fig. 1. It is therefore very difficult to judge the actual decomposition start as deviation from the baseline and this is the reason for the very large estimated uncertainties of ± 20 K or more shown in the first three lines of Table 4. In Fig. 1 the decomposition start is marked by arrows, however, it was not read from this small figure but from the enlarged figure of the digitally recorded signal. The start-criterion was when the deviation from the baseline became larger than the resolution limit of about 0.01 mass%. Even considering this large uncertainty the first heating of the pure GaN powder gives consistently lower temperatures than those samples which consisted of GaN+Ga (2nd–4th heating cycle in Fig. 1). This difference is a clear fact since the large uncertainty of ± 20 K applies to the absolute start temperature but not to the relative values because the same judgment procedure was used for all mass loss curves. The mass loss curve corresponding to this first step decomposition has a slightly different shape compared to the later heating cycles. Around 1273 K there is even a point of inflection. This behavior is resolved in more detail in the following experiment.

This change in the decomposition rate is much more obvious in the mass loss curve for the 24 h isothermal experiment, revealing two stages of decomposition in Fig. 2. The starting temperature of the mass loss is at 1085 K. It is higher than in the first heating cycle of the dynamic method, because the heating rate was 10 K/min instead of 1 K/min. That is also the reason for the higher uncertainty of ± 40 K. The mass loss starts with a high rate around 10%/100 min in the steeper part of Fig. 2 (80–160 min) and drops down to a small value around 1.5%/100 min after an elapsed time of about 200 min. The extrapolation of the slow-rate curve to a theoretical starting point gives a

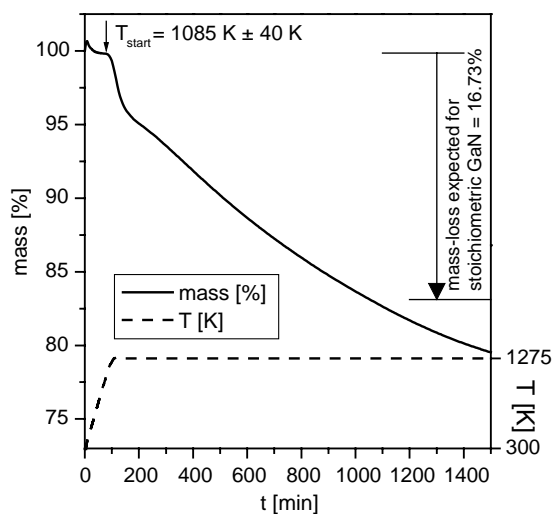


Fig. 2. The mass loss observed for a GaN powder sample heated up to 1275 K and kept at that temperature for 24 h. The starting temperature of the mass loss is higher than in the first heating cycle of the dynamic method, because the heating rate is 10 times higher than in Fig. 1.

Table 4
Results of decomposition of GaN powder from TGA under flowing N_2 at 1 bar

Conditions	Heating	Decomp. start T [K]
GaN, Dynamic oscillation TGA, first heating cycle	First	1043 ± 20
GaN, fast heating TGA (in ramp before 1275 K, 24 h)	First	1085 ± 40^a
GaN (+ in situ Ga) Dynamic oscillation TGA, heating cycles no. 2–4, average value from two samples	Repeated	1135 ± 25
GaN (+ in situ Ga) Isothermal stepping TGA, samples #1, #2, #3, assessed value	Repeated	1110 ± 10

^a Heating rate of 10 K/min instead of 1 K/min.

difference about 2.0 ± 0.5 wt% at T_{start} . This mass loss in the first stage cannot be due to the expected N-release. It is, however, in the same order of magnitude as the measured oxygen contamination (1.44 wt% O) of the samples and may be due to this oxygen release. Also, this first stage is only visible in the first cycle of the dynamic oscillation TGA experiments, the dramatic drop of decomposition rate cannot be observed in any of the following cycles.

In the final stage of the experiment shown in Fig. 2, beyond about 1000 min, the mass loss continues with an only slightly decreased rate. This is observed in all samples, the mass loss did not come to an end even for heating times up to 24 h at relevant temperatures above 1250 K. After sufficient time the measured mass loss goes up to 25%, which is much higher than the 16.73 wt% N expected for stoichiometric GaN. A subsequent nitrogen-analysis of the residual by inert gas fusion gave only 0.77 wt% N, so the actual GaN decomposition was rather complete. The GaN sample kept for 24 h at 1275 K lost 19.73% weight (Fig. 2), the corresponding pure Ga sample lost only 0.75% after the same treatment. It cannot be excluded, though, that the final stage mass loss is nonetheless due to Ga-evaporation since the exposed surface area of Ga in the mixed GaN + Ga sample is probably larger compared to the appearance of the simple sphere of the pure Ga droplet.

A typical mass loss curve for isothermal stepping TGA is presented in Fig. 3. For all samples there can be found a mass gain below and a mass loss above a distinct temperature. For each isothermal step the mass change curves are virtually linear with time. The values of mass change in the central 100 min of each 120 min segment are indicated in Fig. 3 by arrows and numbers.

These values of mass change rate (in %/100 min) are compiled in Fig. 4 for all three samples and all steps up to 1275 K. It should be noted from the linear behavior in Fig. 4 that the mass change rate is related exponentially to temperature. The two lines are evaluated separately for mass gain and mass loss. They are crossing at a temperature of 1110 K and a mass change rate of 0.01%/100 min,

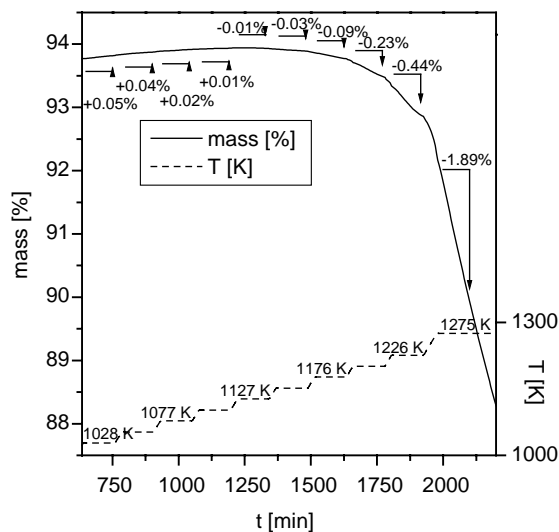


Fig. 3. Typical isothermal stepping TGA curve showing the mass change of a GaN + (Ga) powder sample under N_2 at 1 bar. Not shown is the initial heating cycle up to 1323 K which produced in situ some metallic gallium in the sample from pure GaN.

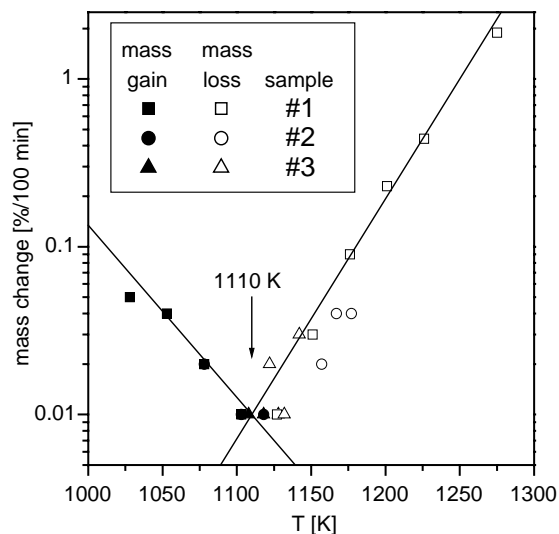


Fig. 4. The change of mass observed in the isothermal-stepping TGA method (see Fig. 3) during the middle 100 min of each 120 min isothermal steps for three different samples. The solid lines are used to find the supposed equilibrium temperature of 1110 K, where the lines for mass gain and mass loss intersect.

which is close to the detection limit. It is of course impossible to extrapolate to “zero loss rate” in Fig. 4 because of the logarithmic scale. This

gain/loss intersection, evaluated at 1110 ± 10 K from Fig. 4, corresponds to both, the decomposition start temperature of GaN at 1 bar N₂ pressure, and to the end temperature of mass gain presumably due to formation of GaN. These are special conditions because of the huge surface area of the intimately mixed powder, compared to a GaN film, and also because of the presence of the liquid metal Ga, known to be a catalyst [22]. It is thus suggested to represent the equilibrium decomposition of GaN, specifically the temperature of the three-phase equilibrium liquid + solid GaN + gas, T^{LSG} .

3. Thermodynamic assessment of the Ga–N system

3.1. Assessment strategy

In order to arrive at internally consistent data for the Ga–N system which comply with the rules of thermodynamics the following steps will be taken:

- (1) Determination of the heat capacity function of GaN, $C_p(T)$, from direct experimental data and derivation of the absolute entropy.
- (2) Selecting a pair of values for absolute entropy and enthalpy of formation of GaN, which determines T^{LSG} at 1 bar. This also determines T^{LSG} with reasonable accuracy for pressures up to 100 bar and temperatures up to 1300 K, where the liquid phase still consists of virtually pure Ga and the fugacity is only 3% higher than the pressure.
- (3) Estimation of the entropy of melting of GaN from systematic trends in other III–V compounds.
- (4) Assessing the melting temperature of GaN from the same systematic trends and from experimental high pressure data on GaN crystal stability and the nitrogen solubility in liquid Ga.

On that basis a consistent thermodynamic model of the Ga–N system is developed and the equilibrium phase diagrams in the entire temperature, pressure and composition range are calcu-

lated. This strategy is a modification of the classical Calphad approach where an optimization of model parameters would have been made by a least square fit to the selected entity of experimental data. This modification is reasonable since the stepwise strategy provides a more direct perception of the individual quantities in this case. The basic idea of the Calphad approach is realized by producing internally consistent sets of Gibbs energy functions of all phases in the Ga–N system which are compared to the entity of experimental data.

It is indispensable to incorporate reliable data on the fugacity–pressure relation of nitrogen. These are developed in the next section.

3.2. Fugacity of nitrogen

If the pressure P is replaced by the fugacity f the thermodynamic equations for the ideal gas describe also the behavior of real gases, specifically in the Gibbs energy

$$G^{\text{gas}} = G^{0,\text{gas}}(T, 1 \text{ bar}) + RT \ln(f/\text{bar}) \quad (1)$$

where R is the gas constant. It will be shown that for high pressures encountered during GaN decomposition f can be several orders of magnitude higher than P .

The equation of state of a real gas can be given in virial form [38]

$$PV = RT + B/V + C/V^2 + D/V^3 + \dots, \quad (2)$$

where V is the molar volume, and B, C, D, \dots are the second, third, forth, \dots virial coefficients. This allows the calculation of the fugacity, f , in the third-term approximation following the approach of Perrot, but mending the misprint [39]:

$$RT \ln \frac{f}{P} = \int_0^P \left(V - \frac{RT}{P} \right) dP, \quad (3a)$$

$$RT \ln f = RT \ln P + \frac{BP}{RT} + \frac{1}{2} \left(C - \frac{B^2}{RT} \right) \left(\frac{P}{RT} \right)^2. \quad (3b)$$

Tsonopoulos [40] gives the following empirical correlation for the temperature dependence of the second virial coefficient $B' = B/RT$:

$$B' \frac{P_c}{RT_c} = \phi^{(0)}(T_R) + \omega \phi^{(1)}(T_R), \quad (4a)$$

$$\phi^{(0)}(T_R) = 0.1445 - 0.330/T_R - 0.1385/T_R^2 - 0.0121/T_R^3 - 0.000607/T_R^8, \quad (4b)$$

$$\phi^{(1)}(T_R) = 0.0637 + 0.331/T_R^2 - 0.423/T_R^3 - 0.008/T_R^8, \quad (4c)$$

$$\omega = -\log_{10} \left(\frac{P^0}{P_c} \right)_{T_R=0.7} - 1.000, \quad (4d)$$

where P_c and T_c are the critical pressure and critical temperature, respectively. Values for N_2 are $P_c = 33.958$ bar, $T_c = 126.192$ K [41]; T_R is the reduced temperature $= T/T_c$, and P^0 is the vapor pressure of nitrogen at $T = 0.7T_c$. The acentric factor ω for N_2 is 0.04 [42]. Because of its simplicity this empirical correlation of Tsonopoulos in the linear approximation of Eq. (3b) is implemented in some commercial thermodynamic software packages to calculate the fugacity coefficient f/P . It will be shown in the following that these approximate calculations which are very useful around the critical temperature and pressure [40] cannot be used in the high pressure/temperature range relevant for GaN decomposition.

Jacobsen et al. [43] performed a comprehensive collection of experimental data about nitrogen properties from the freezing line up to 2000 K and for pressures up to 10 kbar and selected an equation of state. The 28 coefficients were determined by a weighted least square fit to selected data. This equation of state from [43] is used by the freeware program ALLPROPS¹ [44] to calculate and extrapolate the fugacity coefficient f/P , and other nitrogen properties, up to 3000 K and 20 kbar. However, no explicit access to a function $f=f(P)$, necessary for our phase diagram calculations, is given. Such a function will be derived in the following using the experimentally supported data of $f=f(P)$ provided by ALLPROPS.

The function developed here follows the general approach of virial coefficients in Eq. (3b). The fugacity coefficient as function of pressure and

temperature may be generalized to:

$$\ln(f/P) = b'P + c'P^2 + d'P^3$$

$$b' = \frac{b_1}{T} + \frac{b_2}{T^2} + \frac{b_3}{T^3} + \frac{b_4}{T^4},$$

$$c' = \frac{c_1}{T} + \frac{c_2}{T^2} + \frac{c_3}{T^3} + \frac{c_4}{T^4}. \quad (5)$$

The coefficients are determined by a least square fit. In the temperature range 300–2000 K and the pressure range up to 10 or 20 kbar the P^3 term and the fourth order in temperature turned out to be unimportant. These terms were set to zero ($d' = b_4 = c_4 = 0$) in the final adjustment

$$\ln\left(\frac{f}{P}\right) = \left(\frac{0.3926 \text{ K}}{T} - \frac{39.23 \text{ K}^2}{T^2} + \frac{2800 \text{ K}^3}{T^3} \right) \frac{P}{\text{bar}}$$

$$+ \left(-\frac{3.805 \times 10^{-6} \text{ K}}{T} + \frac{0.00113 \text{ K}^2}{T^2} - \frac{0.07 \text{ K}^3}{T^3} \right) \frac{P^2}{\text{bar}^2} \quad (T > \approx 300 \text{ K}). \quad (6)$$

The good agreement of Eq. (6) with the experimental data of [43], calculated by ALLPROPS, is demonstrated in Figs. 5 and 6, shown by the solid line at 300 and 2000 K. The agreement is similarly well for all intermediate temperatures. Above 10 kbar the density of “experimental” data is reduced to indicate that data in this range are calculated by an extrapolation in ALLPROPS. This extrapolation, as well the solid lines calculated from Eq. (6), appears reasonable even well above 10 kbar. Eq. (6) is used for pressures up to 30 kbar; for higher pressures a linear extrapolation in $\ln(f/P)$ —continuous in slope and value at 30 kbar—is used to avoid an artificial maximum produced by the negative value of c' .

In the low pressure range of Fig. 5 a small deviation is visible, the experimental data are below the line calculated from Eq. (6). In fact, the initial slope of the experimental data, which is determined by the second virial coefficient, is even negative. This feature is given correctly by the dashed line calculated after [40], however, at higher pressure that linear approximation in P is completely off. The second virial coefficient, or initial slope, increases with T . It becomes zero at the Boyle temperature (≈ 328 K for N_2) and is positive above that temperature. The discrepancy at 300 K and $P = 70$ bar is $f/P = 1.07$ from Eq. (6)

¹ <http://www.uidaho.edu/~cats/software.htm>

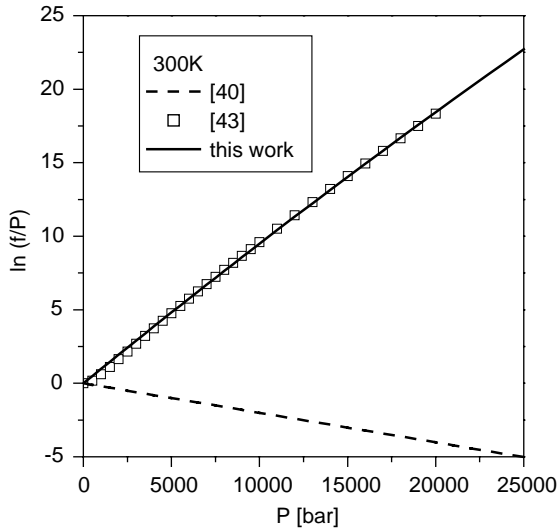


Fig. 5. Fugacity-coefficient of N₂ at 300 K. The squares represent the values calculated by the program ALLPROPS from the experimentally supported equation of state by Jacobsen et al. [43]. The equation by Tsionopoulos [40] should not be used in this pressure range.

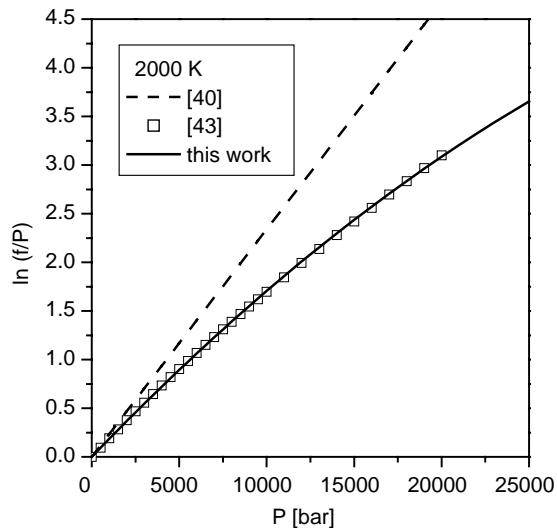


Fig. 6. Fugacity-coefficient of N₂ at 2000 K. Notation like Fig. 5.

compared to $f/P=0.993$ [43]. At such relatively low pressures and especially below room temperature the linear equation [40] is closer to the experimental data than Eq. (6).

At higher pressure it might be tempting to use Eq. (3b) including the P^2 term with $B=B'RT$ from Eq. (4a) [40] and assuming $C=0$; but this gives a correction to the wrong side at low temperature and even at 2000 K, Fig. 6, it is way below the experimental data [43] above 5000 bar, much worse than the linear equation [40]. Therefore the approach of Tsionopoulos [40] cannot be used in the high pressure range relevant here, where f/P deviates dramatically from unity. The present equation (6) is in excellent agreement with the experimental data [43] for temperatures above 500 K even at low pressure. The largest discrepancy is observed at 300 K and $P=1000$ bar with $f/P=2.65$ from Eq. (6) compared to $f/P=1.84$ [43].

Span et al. [41] reviewed the experimental data used by Jacobsen et al. [43] and collected new data, leading to a revised formulation of the equation of state. The comparison between densities and heat capacities calculated with the different equations of state are in good agreement with the data of [43] in the relevant high pressure range.

3.3. Heat capacity and entropy of GaN

Stable GaN crystallizes in the wurtzite (hexagonal) structure with $P6_3mc$ space group. The metastable zinc blende (cubic) crystal structure can also be grown on substrates with cubic symmetry [23]. In the present assessment solid GaN is considered to be a stoichiometric compound in the wurtzite structure. In the key reference on heat capacity [35] the structure of the GaN powder used was also determined to be of the wurtzite type by X-ray diffraction with Rietveld analysis, lattice parameters are $a=0.31891$ nm, $c=0.51853$ nm.

Experimental data on the heat capacity of GaN were given by Demidenko and Koshchenko et al. [32,33], by Yamaguchi, Itagaki et al. [45,46] and by Chen et al. [35]. The C_P measurements of Demidenko and Koshchenko et al. [32,33] were performed with a vacuum adiabatic calorimeter in the temperature range 5–300 K using liquid helium as the cooling agent. Yamaguchi et al. [45,46] used a drop calorimeter ($T_0=298$ K) for sample temperatures from 800 to 1050 K. Chen et al. [35] measured the heat capacity under argon using an

adiabatic scanning calorimeter in the temperature range 113–1073 K. They give no actual data points but report only fitted parameters for an equation of the following form:

$$C_p(T) = A + BT + CT^{-2} + DT^2. \quad (7)$$

For the present low-temperature $C_p(T)$ evaluation and the determination of the absolute value of the standard entropy, S_{298}^0 , the recent recommendation on heat capacity models for non-magnetic crystalline phases [47] is adopted. Essentially, the Debye and Einstein heat capacity models, extended by an empirical term, are fitted to the experimental data, that is

$$C_p(T) = C_{\text{Debye}}(T, \theta_D) + a_D T + b_D T^2 \quad (8)$$

and alternatively

$$C_p(T) = C_{\text{Einstein}}(T, \theta_E) + a_E T + b_E T^2. \quad (9)$$

The empirical constants a and b are used to take care of necessary corrections to the Debye and Einstein models, including the difference $C_p - C_v$. The set of three parameters (θ_D, a_D, b_D) , or alternatively (θ_E, a_E, b_E) , is determined by a simultaneous least square fit of Eqs. (8) or (9) to the experimental data.

The standard entropy, S_{298}^0 , is then determined by numerical integration of $C_p(T)/T$. Independent experimental values of S_{298}^0 , which are sometimes given from cross-reactions with other compounds, are not available for GaN and cannot be incorporated. The philosophy of this entire assessment is to use available experimental data directly and not to use tabulated data from standard references, which may be based on older, less well defined experiments or even estimations. For example, the reported standard entropy of formation of GaN, $\Delta_f S^0 = -135.7 \text{ J/mol K}$ [34] may be recalculated to a standard entropy, $S_{298}^0 = 19.2 \text{ J/mol}$. That value was not used since it was originally derived from the $\log(P_{\text{N}_2})$ vs. $1/T$ data given by Karpinski and Porowski [34], and these data were considered directly in a later stage of the present assessment.

The experimental C_p -data below 300 K are given in Fig. 7b. Below 150 K there is a significant difference between the data of Chen et al. [35] and those from Demidenko and Koshchenko et al.

[32, 33]. It also turned out impossible to fit Eqs. (8) or (9) reasonably well to any of these low temperature data. A set of selected data points is therefore combined to allow an optimization.

According to Chase et al. [47] it is very unusual for the parameters a_D and a_E to be negative, thus they were constrained to be greater than or equal

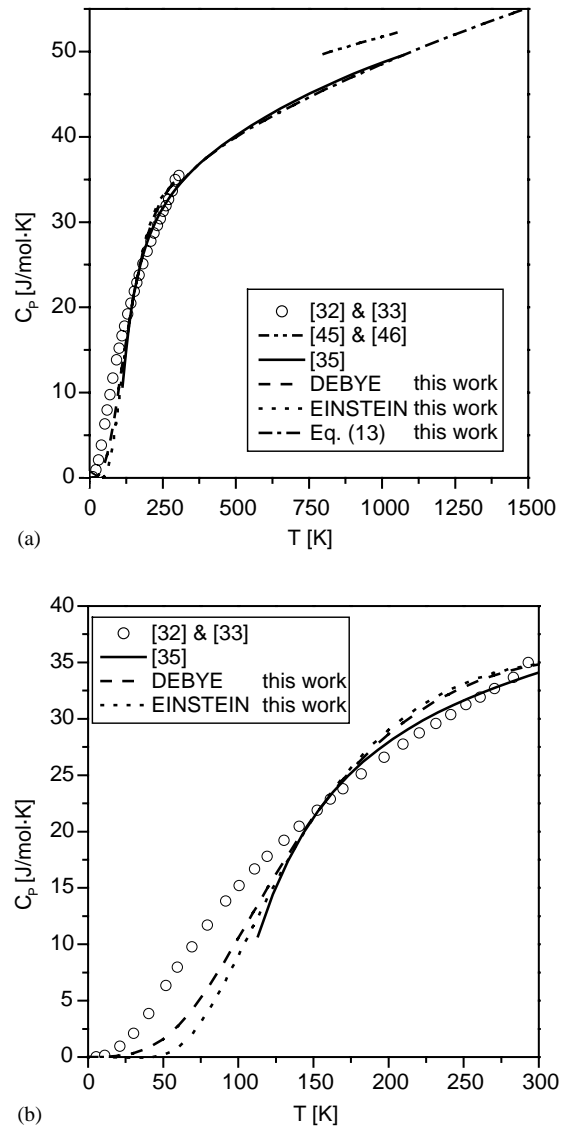


Fig. 7. Heat capacity, C_p , of GaN. (a) Full assessed temperature range [32,33,35]. (b) Enlarged range 0 to 298 K [32,33,35,45,46]. The mol refers to a formula unit of GaN throughout this work.

zero. The optimized values for the Debye and Einstein temperatures and parameters are: $\theta_D = 654$ K, $b_D = -5.524 \times 10^{-5}$ J/mol K³ and $\theta_E = 480$ K, $b_E = -6.207 \times 10^{-5}$ J/mol K³ with $a_D = 0$ and $a_E = 0$. The corresponding curves are compared in Fig. 7a and b to the experimental data. Using these model curves for the numerical integration, the values obtained for S_{298}^0 are 30.4 J/mol K (Debye model), and 28.4 J/mol K (Einstein model). The difference between these models, 2.0 J/mol K is instructive for an estimation of the error contribution from the low temperature part in addition to the experimental error of C_p , reported as less than 1.5% [33].

Both models, Debye and Einstein, are limited in this case to lower temperatures because of the rather high influence of the parameters b_D and b_E around room temperature and above. The more sophisticated Debye model gives higher but probably more realistic values of $C_p(T)$. This model is used up to 155 K, above that the equation from [35] is used for the final determination of S_{298}^0 . The result is $S_{298}^0 = 30.0$ J/mol K with an estimated error of ± 4 J/mol K, as detailed in Eqs. (10)–(12)

$$C_p(T) = C_{\text{Debye}}(T, \theta_D) - 5.524 \times 10^{-5} (T/K)^2 \quad (J/mol K) (0 K < T < 155 K), \quad (10a)$$

$$C_{\text{Debye}}(T, \theta_D) = 18R \left(\frac{T}{\theta_D} \right)^3 \int_0^{\theta_D/T} \frac{x^4 e^x}{(e^x - 1)^2} dx, \quad (10b)$$

$$\theta_D = 654 \text{ K}, \quad (10c)$$

$$C_p = 30.309 + 2.52 \times 10^{-2} T - 2.85593 \times 10^5 T^{-2} - 6.523 \times 10^{-6} T^2 \quad (J/mol K). \quad (155 K < T < 298 K), \quad [35] \quad (11)$$

$$S_{298}^0 = 30.0 \pm 4 \text{ J/mol K}. \quad (12)$$

The mol refers to the formula unit GaN, producing the factor $2 \times 9 = 18$ in Eq. (10b).

The general empiric equation (7) with the parameters from [35], Eq. (11), is not useful beyond the temperature range of the experimental data ($113 \text{ K} < T < 1073 \text{ K}$) because C_p reaches a

maximum around 2000 K and decreases at higher temperatures. With a slight adjustment of parameters in Eq. (11) it can be used in the temperature range from 298 K up to 4000 K without such artifacts. The resulting difference between the original and the adjusted following equation is below 1% in the entire experimentally supported range, as demonstrated in Fig. 7a

$$C_p = 32.532 + 1.867 \times 10^{-2} T - 3.307 \times 10^5 T^{-2} - 2.335 \times 10^{-6} T^2 \quad (J/mol K) \quad (298 \text{ K} < T < 4000 \text{ K}). \quad (13)$$

The experimental data of Yamaguchi and Itagaki et al. [45,46] give a higher C_p compared to those of Chen et al. [35] as shown in Fig. 7a. The latter data are accepted in the present assessment not only because of the much larger temperature range studied but also because Chen et al. [35] performed a careful structural analysis of their samples.

After completion of the present work new data on the heat capacity of GaN were given by Leitner et al. [48]. The heat capacity and the heat content of GaN were measured in the range of 320–570 K and 670–1270 K, respectively. The derived temperature dependence of the heat capacity gives values similar to those of Yamaguchi and Itagaki et al. [45,46]. The data of Chen et al. [35] and also Eq. (13) is at the lower edge of the error range given by Leitner et al. [48]. At 320 K the difference becomes very small, suggesting that C_p below room temperature is not affected, which also applies to the assessed value of S_{298}^0 of Eq. (12).

3.4. Thermodynamic modeling of phase equilibria

In the thermodynamic modeling a Gibbs energy function is assessed for each of the four phases gas, liquid, solid Ga and solid GaN appearing in the Ga–N system. The Gibbs energy function $G_i^{0,\phi}(T) = G_i^\phi(T) - H_i^{\text{SER}}$ for the pure element i ($i = \text{Ga, N}$) in the ϕ phase ($\phi = \text{gas, liquid, or solid orthorhombic Ga}$) is described by the equation:

$$G_i^{0,\phi}(T) = a + bT + cT \ln T + dT^2 + eT^3 + fT^{-1} + gT^7 + hT^{-9}, \quad (14)$$

where H_i^{SER} is the molar enthalpy of the stable element reference (SER) at 298.15 K and 1 bar,

and T is the absolute temperature. The Gibbs energy functions for Ga and N are taken from the SGTE compilation by Dinsdale [49], however, the value of hypothetical liquid N reference state has to be modified, as detailed later. The Gibbs energies of the solid and liquid phases in the Ga–N system were assumed to be pressure independent, since no data are available especially on the molar volume difference of solid and liquid GaN. No solid solubilities are assumed in Ga and GaN.

The binary compound GaN is modeled as stoichiometric phase and the Gibbs energy per mol of formula unit is given by the following expression:

$$G^{\text{GaN}} = G_{\text{Ga}}^{0,\text{orthorh}}(298.15 \text{ K}) + 0.5G_{\text{N}_2}^{0,\text{gas}}(298.15 \text{ K}) + A + BT + CT \ln T + DT^2 + ET^{-1}. \quad (15)$$

The parameters A , B , C , D , and E are determined as follows. From $C_p(T)$ in Eq. (13) the values of C , D , and E and from S_{298}^0 in Eq. (12) the parameter B are given. Finally, A is related to the standard enthalpy of formation, $\Delta_f H_{298}^0 = -156.8 \pm 16 \text{ kJ/mol}$ [36].

These selections, however, are in conflict with the experimental data on phase stability, they

result in $T^{\text{LSG}} = 1286 \text{ K}$ at 1 bar in contrast to the present experimental value of $1110 \pm 10 \text{ K}$. They are also off at higher pressure and it is thus necessary to change the values for $\Delta_f H_{298}^0$ and S_{298}^0 within the given error range. The final setting of parameters A and B in the first line of Table 5 achieves a compromise between these three quantities as given in Table 6. It should be noted that there is no much room for arbitrary choices since all three values of that final assessment, $\Delta_f H_{298}^0$, S_{298}^0 and T^{LSG} , are at the edge of their experimental error bars.

Only few experimental observations were made on liquid Ga–N solutions. It is therefore advisable to use the simplest possible model for the liquid solution phase. This is the disordered substitutional solution model with only one parameter, the regular solution. The molar Gibbs energy is expressed by the following equation:

$$G^{\text{L}} = (1-x)G_{\text{Ga}}^{0,\text{L}} + xG_{\text{N}}^{0,\text{L}} + RT[x \ln x + (1-x) \ln(1-x)] + x(1-x)L_{\text{Ga,N}}^{0,\text{L}} \quad (16)$$

in which x is the atomic fraction of N. $G_{\text{N}}^{0,\text{L}}$ denotes the Gibbs energy of a hypothetical liquid N reference state [49,51]. This value was found to

Table 5
Thermodynamic model parameters for the Ga–N system assessed in this work

Parameters (J/mol)
$G^{\text{GaN}} = -151,618 + 199.209T - 32.532T \ln(T) - 9.335 \times 10^{-3}T^2 + 3.892 \times 10^{-7}T^3 + 165,350T^{-1}$
$L_{\text{Ga,N}}^{0,\text{L}} = -4958 + 4.627T$
$G_{\text{N}}^{0,\text{Liquid}} - 0.5 \cdot G_{\text{N}_2}^{0,\text{gas}} = 63,320 + 59.02T^a$

^aThis value is 33,370 J/mol more positive than that of Dinsdale [49] for metastable liquid nitrogen, see also [50].

Table 6
Important thermodynamic quantities of GaN calculated from the thermodynamic description of Table 5 and the properties of pure stable elements [49]

Quantity	Calculated value	Experimental value	Reference
Standard enthalpy of formation, $\Delta_f H_{298}^0$	-140 kJ/mol	-156.8 ± 16 kJ/mol	[36]
Standard absolute entropy, S_{298}^0	26 J/mol K	30 ± 4 J/mol K	This work
Decomposition temperature, T^{LSG} , at 1 bar	1117 K	1110 ± 10 K	This work
Entropy of melting, $A_m S$	67.4 J/mol K		
Congruent melting temperature, T_m	2700 K		

be not positive enough to enable the stability of GaN up to the assessed congruent melting temperature. It was modified as given in Table 5 by using a similar shift as detailed in a recent thermodynamic analysis of the In–N system [50].

In a proper treatment that constant shift for the hypothetical liquid N reference state should be replaced by a pressure dependence of the Gibbs energy. However, the equation of state is not well known for liquid Ga (certainly not in the high pressure range), it is not at all known for liquid GaN, not to speak of hypothetical liquid N. Using crude empirical volume–pressure relations a rough estimation can be given at a pressure of 93 kbar for an increase in Gibbs energy of +90 kJ/mol for liquid Ga and +50 kJ/mol for GaN, which, together with the +33 kJ/mol for liquid N, retains the liquid–solid–gas equilibrium at the congruent melting point of GaN. This indicates that the constant shift used here has the correct sign and order of magnitude.

The interaction parameter $G_{\text{Ga,N}}^{0,\text{L}}$ is taken to be linearly temperature dependent and is determined at the congruent melting point, using:

$$G^{\text{L}} = G^{\text{GaN}} \quad (\text{at } T_m, x = 0.5) \quad (17)$$

or

$$H^{\text{L}} = H^{\text{GaN}} + \Delta_m H(\text{GaN}), \text{ and} \\ S^{\text{L}} = S^{\text{GaN}} + \Delta_m S(\text{GaN}) \quad (\text{at } T_m, x = 0.5), \quad (18)$$

where T_m , $\Delta_m H$, and $\Delta_m S$ are the melting temperature, enthalpy and entropy, respectively. The enthalpies, H , and entropies, S , of GaN and liquid are determined by standard relations from Eqs. (15) and (16). The entropy of melting is taken from a systematic comparison for all III–V compounds [50] to be $\Delta_m S = 67.4 \text{ J/mol K}$. The melting temperature is estimated from (i) the same systematic comparison, (ii) the lower experimental limit $T_m > 2573 \pm 100 \text{ K}$ from high pressure crystal stability [17], and (iii) from the agreement of the calculated solubility limit, shown in Fig. 8, with experimental data. The finally assessed value of $T_m = 2700 \text{ K}$ agrees with all three constraints and the resulting value of $G_{\text{Ga,N}}^{0,\text{L}}$ is given in Table 5. It is also in reasonable agreement with the melting point at 2791 K predicted from the semi-empirical theory of electronegativity [53].

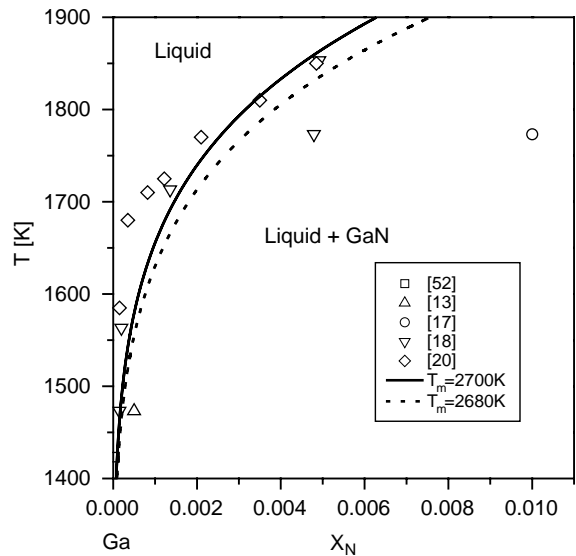


Fig. 8. Experimental data on the solubility limit (liquidus data) in the Ga–N system [13,17,18,20,52]. The lines are calculated using two different assumptions on the congruent melting point of GaN. The solid line corresponds to the thermodynamic data of Table 5.

The gas phase is described as a real gas mixture of the species Ga, Ga₂, N, N₂, and N₃, and its Gibbs energy per total mol of species in the gas is given by following expression:

$$G^{\text{gas}} = \sum y_i [G_i^{0,\text{gas}} + RT \ln(y_i)] + RT \ln(f/\text{bar}), \quad (19)$$

where y_i is the mole fraction of species i in the gas in internal equilibrium, and f is the fugacity of the gas, which becomes identical to the pressure, P , at low P . In the Ga–N system it was found by the present calculations that in the entire pressure–temperature range below 1000 bar and 1500 K the fugacity of N₂ is not much different from its pressure and that the gas consists of virtually pure N₂, any other species occurring with molar fractions below 10^{−7}. This is supported by the finding that the equilibrium partial pressure of Ga vapor in the system is much lower than the corresponding N₂ pressure [54]. It is therefore a reasonable approximation to use Eq. (19) with the fugacity–pressure relation of N₂ only instead of the partial fugacities of the individual species, which are unknown anyway. The Gibbs energy

functions $G_i^{0,\text{gas}}(T, 1 \text{ bar})$ of the individual gas species were taken from [55] (for Ga, Ga₂, N and N₃) and from [49] (for N₂).

The thermodynamic equilibrium and phase diagram calculations in the Ga–N system were done by minimizing the total Gibbs energy, using the Pandat program [56].

4. Discussion

Fig. 9 shows the calculated phase stability diagram of the Ga–N system. It should be noted that only the experimental data at 1 bar, and in a small adjustment up to 100 bar, have been used to determine the thermodynamic model parameters. The main part of the calculated curve, especially at higher pressure, is a prediction from the consistent thermodynamic model.

The experimental solid symbols on the right part of the legend denote stable crystalline GaN (with

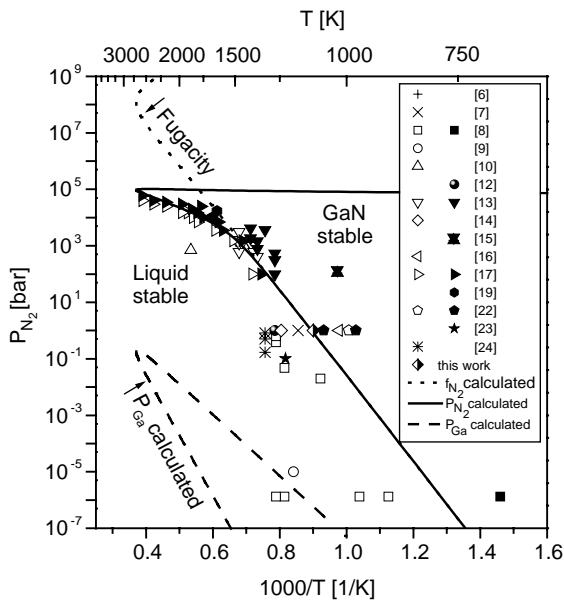


Fig. 9. Phase stability diagram showing the three-phase equilibrium liquid + solid GaN + gas, T^{LSG} [6–10,12–17,19,22–24]. In the lower part the calculated vapor pressure of gallium, P_{Ga} , is superimposed. The solid symbols on the right part of the legend denote experimentally found stable GaN, those on the left part denote GaN decomposed into liquid + gas. The calculated lines corresponds to the thermodynamic data of Table 5.

gas), the open symbols on the left part denote that GaN is decomposed into liquid + gas. The dotted curve extending to the temperature maximum at 2700 K and $f_{\text{N}_2} \approx 10^8$ bar shows the three-phase equilibrium liquid + solid GaN + gas with the fugacity of N₂ as the y-axis. This curve is a virtually straight line from the lowest temperature up to almost the maximum temperature, corresponding to the congruent melting point of GaN. Beyond that it extends in a roughly symmetrical fashion to even higher fugacity, corresponding to nitrogen-rich liquid. This behavior is typical for prototype systems A–B with one congruent melting compound AB and a volatile component B, and for an ideal gas this dotted curve would represent the typical $\log(P_B) - 1/T$ phase stability diagram. This is not the case for real nitrogen. The fugacity coefficient of nitrogen, f/P , grows exponentially to very large values in the high-pressure range and therefore the actual three-phase equilibrium pressure, P_{N_2} , shown by the solid curve, is depressed substantially below the values of f_{N_2} . Beyond the congruent melting point P_{N_2} stays around 10^5 bar with decreasing temperature, corresponding to hypothetical nitrogen-rich liquid.

As stated in the previous section, the global equilibrium calculation shows that N₂ is the dominating species in the gas phase with $y_{\text{N}_2} \approx 1$. The next noticeable minority gas species is elemental gallium and its calculated partial pressure, P_{Ga} , along the three-phase equilibrium is also shown in Fig. 9. It should be noted that for the same Ga-rich liquid one has to read P_{Ga} from the upper part of the dashed P_{Ga} -curve whereas P_{N_2} is read from the lower part of the solid P_{N_2} -curve. The opposite (remote) parts of the P_i curves correspond to hypothetical nitrogen-rich liquid. For Ga-rich saturated liquid at 1250 K P_{Ga} , is more than 6 orders of magnitude below the corresponding value of P_{N_2} .

Fig. 9 can also be viewed as a phase diagram since P_{N_2} is practically identical to the total pressure P . Disregarding the curves of P_{Ga} and the fugacity, the phase field to the left of the solid curve denotes the stability region of the liquid phase, and the phase field to the right denotes the stability region of GaN. All the experimental data shown in Fig. 9 for comparison belong to the

lower part of the P_{N_2} curve, the phase limit between the Ga-rich liquid phase and solid GaN. Experimental details of these data can be found in Table 1. For most data a good agreement with the calculated line is observed.

In the present experiments the limiting temperature between reproducible mass gain and mass loss of GaN (+Ga), 1110 ± 10 K from Fig. 4, is interpreted as the temperature of the three-phase equilibrium liquid+solid GaN+gas, T^{LSG} , at 1 bar N_2 . This is also supported by the similar slope of the gain/loss lines in Fig. 4 around that temperature, indicating a comparable though reversed reaction process. This result of the isothermal stepping TGA method is probably the most accurate value available and it is supported by the independent dynamic oscillation experiments. It is also in agreement with most of the reported data at 1 bar given in Table 1 and Fig. 9. The thin film decomposition experiments of [22] show a lower temperature, however, they were performed with hydrogen addition (5%) to the nitrogen gas. Other data in Fig. 9 which seem to be outside the calculated phase stability limit are those of Morimoto [12] and Tanaka et al. [23] who heated their sample for a rather short time (only 20 and 15 min, respectively). It may be assumed that the rate of decomposition was too small to be detected. In the case of Furtado and Jacob [16] the composition of the atmosphere above the GaN sample is somewhat unclear.

It is interesting to note that similar TGA experiments performed with InN [50] show a mass loss only (> 773 K) but no reproducible mass gain below that temperature. Thus only the decomposition of InN and not the equilibrium value of T^{LSG} could be observed. This is consistent with a comprehensive thermodynamic analysis of the In–N system indicating that the actual equilibrium T^{LSG} at 1 bar is well below room temperature (243 K) for InN [50]. Such an extensive metastable range, with InN crystals existing 530 K above equilibrium temperature, is not observed for GaN if the liquid Ga catalyst is present.

The continuing mass loss in the final stage of the present decomposition experiments at 1275 K clearly exceeds the amount of nitrogen in the GaN samples. It may be ascribed to Ga evapora-

tion into the flowing nitrogen atmosphere. This is possibly enhanced by a larger active surface area of the decomposed GaN powder sample residual since, by contrast, the mass loss (evaporation) from an initially pure Ga-droplet is much less. This enhancement would be necessary considering the low calculated vapor pressure of Ga at the three-phase equilibrium, shown in Fig. 9. It is again interesting to compare this behavior to the decomposition experiments of InN, performed under similar conditions [50]. The InN samples show a sharp stop in mass loss after loosing the stoichiometric amount of N even after prolonged tempering at 900 K. It is obvious that the necessarily higher temperature for the GaN decomposition also promotes this effect.

The data on the solubility of nitrogen in the liquid phase were used to determine the final value of the first constant of $L_{Ga,N}^{0,L}$, given in Table 5, by setting the melting temperature of GaN. This determines the enthalpy of melting, Eq. (18), and finally the parameter -4958 J/mol, corresponding to the enthalpy of mixing of the liquid, $-4958/4 = -1240$ J/mol at $x_N = 0.5$. The experimental solubility data are compared to the calculated phase boundary based on $T_m = 2700$ K in Fig. 8. The dotted line in Fig. 8 is added just to show the effect of using an only 20 K lower value of $T_m = 2680$ K, producing also a different value of the parameter $L_{Ga,N}^{0,L}$. It should be noted that some data in the two publications of Grzegory et al. [18,20] seem to be based on the same experiments. Therefore some of the nearest data points in Fig. 8 may be redundant and not independently determined.

Fig. 10 compiles published experimental data on the stability of GaN under NH_3 or mixtures containing NH_3 using the partial pressure of ammonia, P_{NH_3} , as axis. We do not follow the suggestion of Thurmond and Logan [28] to calculate a theoretical partial pressure of nitrogen from each individual data point of (P_{NH_3}, T) using the reaction equation



Very large values of P_{N_2} would be produced by that calculation, but they are based on the assumption that the ratio $P_{N_2}^{0.5} P_{H_2}^{1.5} / P_{NH_3} = K$

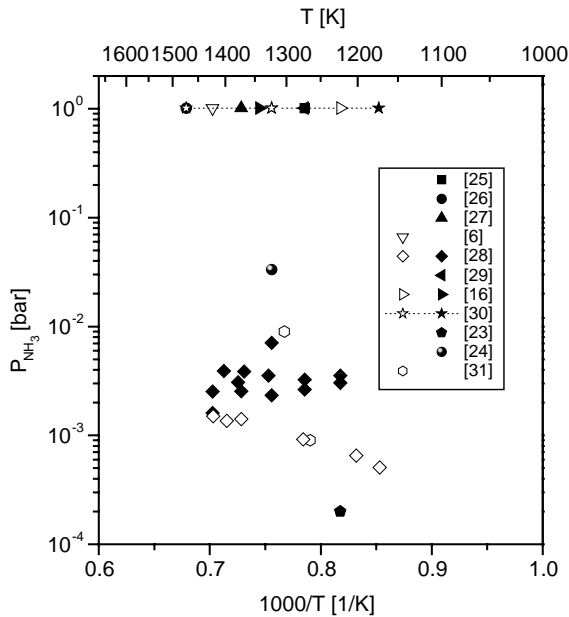
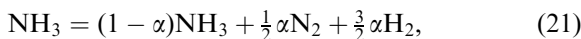


Fig. 10. Experimental data from literature on the stability of GaN under NH_3 or mixtures containing NH_3 , see Table 2 for experimental conditions. Notation used for solid/open symbols like Fig. 8.

remains constant at given T . However, once the dissociation according to Eq. (20) actually occurs in a given stream of NH_3 (+carrier gas) at atmospheric pressure in the furnace, the value of P_{NH_3} will drop and the chemical equilibrium of Eq. (20) will be attained at small values of P_{NH_3} and less than atmospheric pressure of P_{N_2} . The kinetic constraint of the NH_3 decomposition in open systems may be considered according to the reaction



where measured values of α are 0.1 or less under typical growth conditions [57].

Therefore such theoretically calculated very large values of P_{N_2} from Fig. 10 are not used or superimposed to Fig. 9. It remains a fact, though, that the presence of ammonia — or better hydrogen — has its impact on the stability and formation of GaN, as also seen from the data of Pisch et al. [22] in Fig. 9. In the pure binary Ga–N system the stability data are internally consistent in the entire low- and high-pressure range as discussed before with Fig. 9. So there is no need to

add any recalculated data of Fig. 10, which are obviously not internally consistent as visualized by the solid (stable) and open (decomposed) symbols. The impact of hydrogen on the decomposition of GaN was also discussed by L'vov [58].

Based on the same assessed thermodynamic data in Table 5 the phase diagrams at 1 bar total pressure, Fig. 11, and also the condensed phase diagram with the gas phase suspended, Fig. 12, are calculated. In Fig. 11 also the experimental data at 1 bar nitrogen, the same as those in Fig. 9, are superimposed. Under these conditions the solubility of N in liquid Ga is too small to be visible in Fig. 11, the maximum value is $x_{\text{N}} = 1.7 \times 10^{-5}$ at 2270 K. The solubility at $T^{\text{LSG}} = 1117$ K is only $x_{\text{N}} = 9 \times 10^{-7}$. Fig. 12 shows the congruent melting of GaN and some isobars of P_{N_2} (or P) are given for the two-phase equilibrium Ga-rich liquid + GaN, consistent with Fig. 9. The nitrogen rich part of the liquidus line is of course hypothetical. A more complex modeling of the liquid phase, e.g. with a liquid miscibility gap, may also be applied, however, the simplest possible model for the liquid solution phase used here, Table 5, gives a

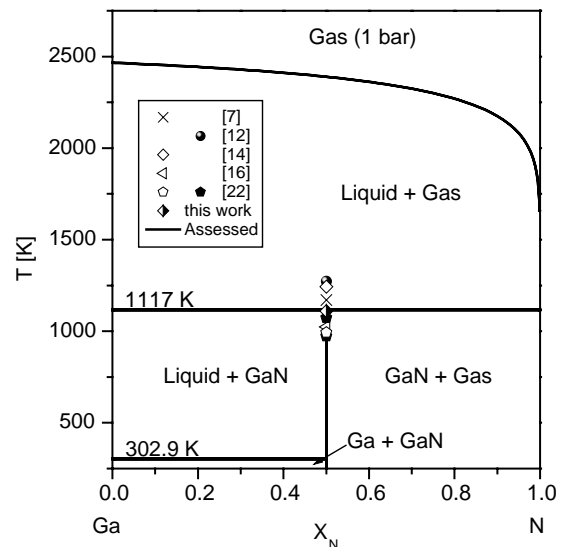


Fig. 11. Section of phase diagram at 1 bar pressure. Above 1117 K GaN decomposes into liquid and gas, virtually pure gallium and N_2 , respectively. Experimental data are superimposed. Solid symbols denote solid GaN, open symbols denote GaN decomposed into liquid+gas. The calculated phase diagram corresponds to Table 5.

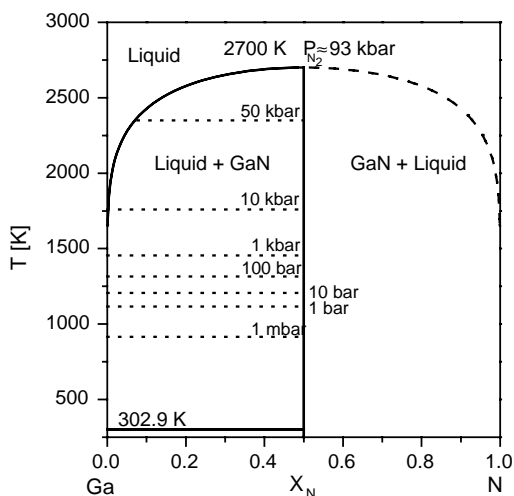


Fig. 12. Calculated condensed phase diagram of the Ga–N system, corresponding to Table 5. Equilibrium isobars of pressure P are superimposed.

satisfactory description of all experimental data without producing unreasonable artifacts in the extrapolated regions.

The most carefully conducted direct measurement of the standard enthalpy of formation of Ranade et al. [36] supersedes the early work of Hahn and Juza [27] and forms one cornerstone of the present assessment. The other data reported on $\Delta_f H_{298}^0$, Table 3, are not used since they were derived from P – T^{LSG} measurements which are already considered in Fig. 9. These data are nevertheless in agreement, confirming the general consistency of caloric and vapor pressure measurements in the Ga–N system which are not at all given in the related In–N system [50]. The reported standard entropy of GaN, $S_{298}^0 = 36.5(9)$ J/mol K [32,33], Table 3, is larger than the value derived in Eq. (12) simply because the C_p -data of Demidenko and Koshchenko et al. [32,33] below 150 K are much higher than the adjusted Debye-function in Fig. 7b. An extrapolation of the experimental data from Chen et al. [35] below 113 K may suggest an even lower C_p -curve and consequently a lower value of S_{298}^0 . This supports the final assessment of $S_{298}^0 = 26$ J/mol K, at the lower edge of the estimated error bar in Eq. (12). Within the triple of values ($\Delta_f H_{298}^0$, S_{298}^0 and T^{LSG} at 1 bar) only two

could be chosen independently, the third is fixed by that choice. It is emphasized that all three values are finally assessed at the edges of their individual experimental error bars in order to obtain a consistent thermodynamic description of all caloric and decomposition or vapor pressure measurements around 1 bar, as compared in Table 6.

5. Conclusion

- Isothermal stepping TGA enables not only the most precise measurement of the decomposition temperature of GaN, it also shows a reproducible mass gain at slightly lower temperature and thus gives the equilibrium temperature, T^{LSG} , see Table 6.
- Despite some inconsistency in the C_p data of GaN below 150 K a reasonably well established function $C_p(T)$ combined with a value of the absolute standard entropy can be derived, see Eq. (12).
- The final assessment of the triple of values ($\Delta_f H_{298}^0$, S_{298}^0 and T^{LSG} at 1 bar, Table 6) can be made by simple calculations for pressures up to 100 bar and temperatures up to 1300 K, where the liquid phase still consists of virtually pure Ga and the fugacity is only 3% higher than the pressure. In this range the following simplified equation may be used for the equilibrium pressure of the reaction $\text{GaN} = \text{Ga(L)} + \frac{1}{2}\text{N}_2$:

$$\log_{10}(P_{\text{N}_2}/\text{bar}) = 13.569 - 1.516 \times 10^4/(T/\text{K})$$

$$(T < \approx 1300 \text{ K}). \quad (22)$$
- At higher pressure the fugacity becomes several orders of magnitude larger than the pressure. An explicit equation for $f(P)$ is developed, Eq. (6), which is useful for the conversion of complex phase diagram calculation output. This equation is supported by experimental data [43] up to 2000 K and 10 kbar and reasonably extrapolated beyond. It is also shown that the widely accepted approach by Tsonopoulos cannot be used in that range but only for low pressure calculations.
- The assessment of melting properties of GaN (entropy, $\Delta_m S$, and temperature, T_m) is based

on systematic trends of III–V compounds, for T_m also experimental data are used. For the entire liquid phase the most simple solution model was used with only two parameters, determined by $\Delta_m S$ and T_m .

- The entire information assessed in this work is condensed in the thermodynamic model parameters for the Ga–N system, Table 5. Based on that and the properties of the pure elements and gas species all thermodynamic data and phase diagrams are calculated. They indicate a good overall agreement between the different types of experimental data (calorimetric, vapor pressure, phase equilibrium). The consistent assessment is at the edges of the experimental error bars of the key quantities, Table 6. This is different from the related In–N system where a similar analysis reveals fundamental discrepancies.
- The high pressure part of the decomposition pressure of GaN, Fig. 9, is actually predicted from the thermodynamic model in good agreement with the experimental data. It is emphasized that only the data of the purely binary Ga–N system should be used and that the experimental studies involving ammonia should be treated separately.
- Further work is suggested to include a quantitative pressure dependence of the Gibbs energies of solid GaN and the Liquid phase, which were assumed to be similar in the present work.

Acknowledgement

This study was supported by the German Research Council (DFG) under Grant No. Schm 588/23.

References

- [1] S. Strite, H. Morkoç, *J. Vac. Sci. Technol. B* 10 (4) (1992) 1237.
- [2] J.H. Edgar, S. Strite, I. Akasaki, H. Amano, C. Wetzel, *Properties and Applications of Gallium Nitride and Related Semiconductors*, EMIS Datareview Series No. 16, Inspec, London, United Kingdom, 1999.
- [3] S.C. Jain, M. Wilander, J. Narayan, R. Van Overstraeten, *J. Appl. Phys.* 87 (3) (2000) 965.
- [4] A. Davydov, T.J. Anderson, in: T.D. Moustakas, S.E. Mohny, S.J. Pearton (Eds.), *III–V Nitride Materials and Processes III*, Electrochemical Society, Vol. 98–18, Pennington, NJ, 1998, pp. 38–49.
- [5] A.V. Davydov, W.J. Boettinger, U.R. Kattner, T.J. Anderson, *Phys. Stat. Sol. A* 188 (1) (2001) 407.
- [6] R. Juza, H. Hahn, *Z. Anorg. Allg. Chem.* 244 (1940) 133.
- [7] R.J. Sime, J.L. Margrave, *J. Phys. Chem.* 60 (1956) 810.
- [8] M.R. Lorenz, B.B. Binkowski, *J. Electrochem. Soc.* 109 (1) (1962) 24.
- [9] R.C. Schoonmaker, A. Buhl, J. Lemley, *J. Phys. Chem.* 69 (10) (1965) 3455.
- [10] J.B. MacChesney, P.M. Bridenbaugh, P.B. O'Connor, *Mater. Res. Bull.* 5 (1970) 783.
- [11] R. Groh, G. Gerey, L. Bartha, J.I. Pankove, *Phys. Stat. Sol. A* 26 (1974) 353.
- [12] Y. Morimoto, *J. Electrochem. Soc.* 121 (1974) 1383.
- [13] R. Madar, G. Jacob, J. Hallais, R. Fruchart, *J. Crystal Growth* 31 (1975) 197.
- [14] G. Jacob, R. Madar, J. Hallais, *Mater. Res. Bull.* 11 (1976) 445.
- [15] K. Gillessen, K.-H. Schuller, B. Struck, *Mater. Res. Bull.* 12 (1977) 955.
- [16] M. Furtado, G. Jacob, *J. Crystal Growth* 64 (1983) 257.
- [17] J. Karpinski, J. Jun, S. Porowski, *J. Crystal Growth* 66 (1984) 1.
- [18] I. Grzegory, M. Bockowski, J. Jun, P. Figurny, *High Press. Res.* 7 (1991) 284.
- [19] I. Grzegory, J. Jun, S. Krukowski, M. Boćkowski, S. Porowski, *Physica B* 185 (1993) 99.
- [20] I. Grzegory, J. Jun, M. Boćkowski, S. Krukowski, M. Wróblewski, B. Lucznik, S. Porowski, *J. Phys. Chem. Solids* 56 (3/4) (1995) 639.
- [21] O. Ambacher, M.S. Brandt, R. Dimitrov, T. Metzger, M. Stutzmann, R.A. Fischer, A. Miehr, A. Bergmaier, G. Dollinger, *J. Vac. Sci. Technol. B* 14 (6) (1996) 3532.
- [22] A. Pisch, R. Schmid-Fetzer, *J. Crystal Growth* 187 (1998) 329.
- [23] H. Tanaka, A. Nakadaira, *J. Crystal Growth* 189/190 (1998) 730.
- [24] A. Rebey, T. Boufaden, B. El Jani, *J. Crystal Growth* 203 (1999) 12.
- [25] W.C. Johnson, J.B. Parsons, M.C. Crew, *J. Phys. Chem.* 36 (1932) 2651.
- [26] R. Juza, H. Hahn, *Z. Anorg. Allg. Chem.* 239 (1938) 282.
- [27] H. Hahn, R. Juza, *Z. Anorg. Allg. Chem.* 244 (1940) 111.
- [28] C.D. Thurmond, R.A. Logan, *J. Electrochem. Soc.* 119 (5) (1972) 622.
- [29] S.S. Liu, D.A. Stevenson, *J. Electrochem. Soc.* 125 (7) (1978) 1161.
- [30] C.M. Balkaş, R.F. Davis, *J. Am. Ceram. Soc.* 79 (9) (1996) 2309.
- [31] D.D. Koleske, A.E. Wickenden, R.L. Henry, *MRS Internet J. Nitride Semicond. Res* 591 (2000) W 3.64.

- [32] A.F. Demidenko, V.I. Koshchenko, L.D. Sabanova, Yu.M. Gran, *Russ. J. Phys. Chem.* 49 (6) (1975) 940.
- [33] V.I. Koshchenko, A.F. Demidenko, L.D. Sabanova, V.E. Yachmenev, Yu.M. Gran, A.F. Radchenko, *Inorg. Mater. (USA)* 15 (1979) 1329.
- [34] J. Karpinski, S. Porowski, *J. Crystal Growth* 66 (1984) 11.
- [35] X. Chen, Y. Lan, J. Liang, X. Cheng, Y. Xu, T. Xu, P. Jiang, K. Lu, *Chin. Phys. Lett.* 16 (2) (1999) 107.
- [36] M.R. Ranade, F. Tessier, A. Navrotsky, V.J. Leppert, S.H. Risbud, F.J. DiSalvo, C.M. Balkas, *J. Phys. Chem. B* 104 (2000) 4060.
- [37] I.N. Przhevalskii, S.Yu. Karpov, Yu.N. Makarov, *MRS Internet J. Nitride Semicond. Res.* 3 (30) (1998) 1.
- [38] G.N. Lewis, M. Randall, K.S. Pitzer, L. Brewer, *Thermodynamics*, McGraw-Hill Book Company, New York, 1961.
- [39] P. Perrot, *A to Z of Thermodynamics*, Oxford University Press, Oxford, 1998, pp. 318–319.
- [40] C. Tsonopoulos, *AIChE J.* 20 (2) (1974) 263.
- [41] R. Span, E.W. Lemmon, R.T. Jacobsen, W. Wagner, A. Yokozeki, *J. Phys. Chem. Ref. Data* 29 (6) (2000) 1361.
- [42] K.S. Pitzer, D.Z. Lippmann, R.F. Curl, Ch.M. Huggins, D.E. Petersen, *J. Am. Chem. Soc.* 77 (1955) 3433.
- [43] R.T. Jacobsen, R.B. Stewart, M. Jahangiri, *J. Phys. Chem. Ref. Data* 15(2) (1986) 736–794, 814f., 908f.
- [44] E.W. Lemmon, R.T. Jacobsen, S.G. Penoncello, S.W. Beyerlein, *Computer Programs for Calculating Thermodynamic Properties of Fluids of Engineering Interest*, version 6/4/1996, CATS University of Idaho Moscow, USA, 1996.
- [45] K. Yamaguchi, K. Itagaki, A. Yazawa, *J. Jpn. Inst. Metals* 53 (8) (1989) 764.
- [46] K. Itagaki, K. Yamaguchi, *Thermochim. Acta* 163 (1990) 1.
- [47] M.W. Chase, I. Ansara, A. Dinsdale, G. Eriksson, G. Grimvall, L. Höglund, H. Yokokawa, *CALPHAD* 19 (4) (1995) 437.
- [48] J. Leitner, A. Strejc, D. Sedmidubský, K. Růžička, *Thermochim. Acta* 401 (2) (2003) 169.
- [49] A.T. Dinsdale, *CALPHAD* 15 (4) (1991) 317.
- [50] B. Onderka, J. Unland, R. Schmid-Fetzer, *J. Mater. Res.* 17 (12) (2002) 3065.
- [51] K. Frisk, *CALPHAD* 15 (1) (1991) 79.
- [52] R.A. Logan, C.D. Thurmond, *J. Electrochem. Soc.* 119 (12) (1972) 1727.
- [53] J.A. Van Vechten, *Phys. Rev. B* 7 (4) (1973) 1479.
- [54] Z.A. Munir, A.W. Searcy, *J. Chem. Phys.* 42 (12) (1965) 4223.
- [55] *SGTE Substance Database*, Royal Institute of Technology, Sweden, 1994.
- [56] *PANDAT, Software for Multicomponent Phase Diagram Calculation*, Computherm LLC, 437 S. Yellowstone Drive, Suite 217, Madison, WI 53719, USA, 2001.
- [57] M. Ilegems, *J. Crystal Growth* 13/14 (1972) 360.
- [58] B.V. L'vov, *Thermochim. Acta* 360 (2000) 85.